# Plasmonic characteristics in nanoscale graphene resonator-coupled waveguides

**Hua Lu**

**Abstract** In this paper, we numerically and theoretically investigate the propagation of surface plasmon polaritons in a graphene-based resonator-coupled waveguide system, consisting of a monolayer graphene ribbon coupling to two graphene sheets. The resonance wavelength of this system can be easily tuned by adjusting the chemical potential and the width of the graphene ribbon. Both resonance bandwidth and spectral transmission characteristics of the structure strongly depend on the coupling distance and overlap length between the graphene ribbon and graphene sheets. The structural symmetry is found to be another essential parameter. The presented results may pave the way toward the dynamic control of light propagation in graphene-based structures and the realization of tunable graphene-based optoelectronic devices.

## 1 Introduction

Surface plasmon polaritons (SPPs), electromagnetic waves trapped on the metal-dielectric surface and coupled to the free electron oscillations in the metals, are regarded as one of the most promising technologies to realize the ultracompact photonic devices because of the ability to overcome the diffractive limit of light [1, 2]. A large number of SPP

H. Lu (✉)
Centre for Micro-Photonics and CUDOS, Faculty of Science, Engineering and Technology, Swinburne University of Technology, Hawthorn, VIC 3122, Australia
e-mail: luhua@opt.ac.cn

H. Lu
State Key Laboratory of Transient Optics and Photonics, Xi'an Institute of Optics and Precision Mechanics, Chinese Academy of Sciences, Xi'an 710119, China

devices, such as optical switches [3–5], optical buffers [6], wavelength demultiplexers [7], absorbers [8], rulers [9], resonators [10], optical amplifiers [11], filters [12–14], solar cells [15] and sensors [16], have been experimentally demonstrated and numerically simulated. Graphene, a two-dimensional single layer of carbon atoms arranged in a honeycomb lattice, has exhibited many unique and fantastic properties in electronics since its successful fabrication [17, 18]. Recently, optical responses were observed in graphene-based structures such as the optical saturable absorption and broadband polarization [19, 20]. As an overlap between graphene physics and plasmonics, graphene plasmonics (GPs) has attracted extensive attention and been investigated in several graphene architectures [21–27]. GPs is regarded as a promising technology for strong light-matter interactions due to the special behaviors like novel metals [28]. Most importantly, SPPs generated in graphene exhibit the favorable characteristics that make graphene a remarkable alternative to metal-based plasmonics such as extreme electromagnetic confinement, relatively low dissipative loss and dynamic tunability by changing the doping level via the electrostatic or chemical gating [29, 30]. Recently, the manipulation of optical features for GPs has been concentratively studied [11, 22, 24, 28, 31–42]. For example, Vakil et al. [21] found that a flake of graphene with spatial inhomogeneous and nonuniform conductivity patterns acted as a one-atom-thick platform for infrared metamaterials and transformation optical devices. Christensen et al. numerically investigated the plasmonic interaction and hybridization in neighboring aligned ribbons [12]. Wang et al. [31] showed that monolayer graphene arrays possessed fascinating properties of beam control due to the coupling between graphene sheets and proposed the graphene plasmonic coupler [33]. Xu et al. presented that a guided-wave resonance in monolayer

graphene was efficiently excited by an etched diffractive grating on a silicon layer and used to create a sharp notch on the transmission spectrum [32]. Gan et al. [38] numerically and theoretically investigated the excitation of SPPs in doped graphene sheets with a coupling prism and the switching effect in a graphene array [24]. Martin-Moreno et al. showed an interesting propagation and scattering of GPs in the graphene sheet with cracks [39], as well as the influence of the GP reflection phase on graphene ribbon resonators [40]. Chen et al. [41] experimentally demonstrated the plasmonic properties of an epitaxial quasi-free-standing monolayer graphene and found the strong plasmon reflection at the steps between the SiC terraces. These unique features make graphene an excellent candidate for highly tunable plasmonic and optoelectronic devices at terahertz and infrared frequencies.

In this paper, we numerically and theoretically investigate the plasmonic propagation and resonant features in a nanoscale graphene resonator-coupled waveguide. This plasmonic graphene system is composed of two guided-wave graphene sheets coupled with a controllable graphene nanoribbon. It is found that plasmonic resonance and transmission spectral features possess the strong dependence on the chemical potential and width of the graphene ribbon as well as the geometrical symmetry. The coupling strength and overlap length between the graphene ribbon and graphene sheets also determine the transmission spectral response. These results may find potential applications in nanoscale mid-infrared plasmonic and optoelectronic devices, especially wavelength-selective components.

## 2 Structure and model

As shown in Fig. 1a, the proposed graphene system consists of a monolayer graphene nanoribbon and two graphene sheets embedded in dielectric layer (with permittivity $\varepsilon_r$). A small gap $g$ exists between graphene ribbon and graphene sheets. To facilitate effective SPP coupling, an identical overlap length $d$ is set near the two sides of graphene nanoribbon. The graphene nanoribbon width is $W$. In our configuration, the light is only impinged from the left port of the graphene sheet. The highly confined transverse magnetic (TM)-polarized SPP wave will be supported and propagate in the graphene sheet, which acts as a guided-wave element [21]. The monolayer graphene in terahertz and infrared regions can be described with a complex-valued surface conductivity $\delta_g$, which is governed by the Kubo formula [37] containing the intraband and interband contributions. It is related to the chemical potential $\mu_c$, photon frequency $\omega$, reduced Planck's constant $\hbar$, Boltzmann's constant $k_B$ and temperature $T$. In the mid-infrared frequency range, the intraband transition contribution of the
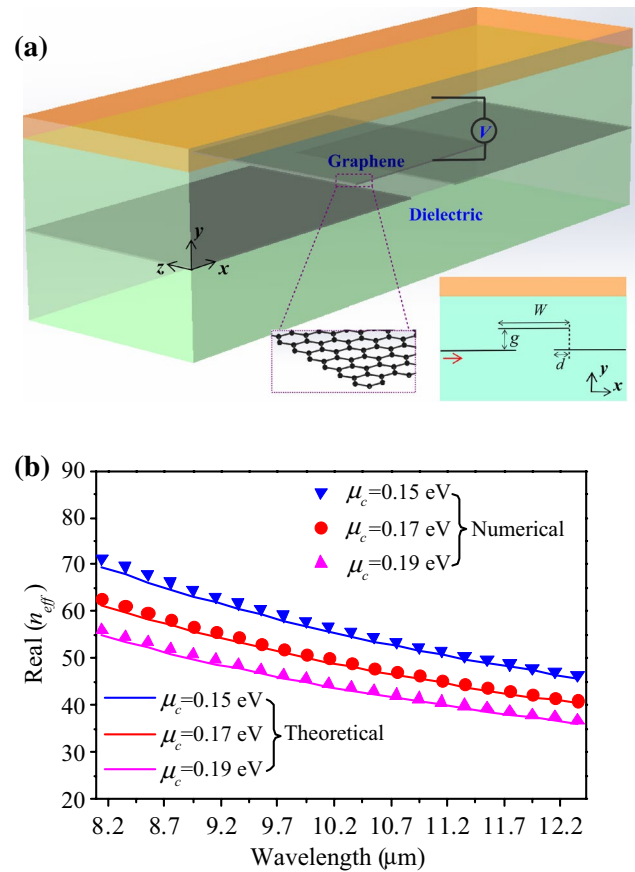


**Fig. 1** **a** Schematic diagram of the graphene-based plasmonic resonator-coupled waveguide system with two graphene sheets and a graphene ribbon. The monolayer honeycomb lattice depicts the microscopic feature of the graphene. The inset shows the cross-section diagram of the graphene structure. The SPP wave is excited from the left port and denoted by the *red arrow*. **b** Theoretical and numerical results of the real part of effective refractive index $n_{eff}$ for the SPP mode supported by the freestanding monolayer graphene with different chemical potentials

graphene dominates [31]. Under the condition of $\mu_c \gg k_B T$, the surface conductivity can be reduced to a Drude-like form [22, 31],

$$\sigma_g(\omega) = \frac{ie^2\mu_c}{\pi\hbar^2(\omega + i\tau^{-1})}. \tag{1}$$

Here, $e$ is the electron charge and $\tau$ stands for the momentum relaxation time due to the carrier intraband scattering. In our study, the physical parameters about the graphene are rationally set as $\mu_c = 0.15$ eV, $T = 300$ K and $\tau = 0.5$ ps [31]. For the purpose of numerical simulation, the graphene is treated as an ultrathin film layer with a thickness of $\Delta$. The equivalent relative permittivity is dependent on the thickness and given by $\varepsilon_g = 1 + i\sigma_g/(\omega\varepsilon_0\Delta)$ [21, 31]. Here, $\Delta$ is not the real thickness of graphene and reasonably set to be 1 nm [21, 31, 32]. For a

**Fig. 2 a** Transmission spectra in the graphene system with $d = 40$ nm, $g = 50$ nm and $W = 200$ nm. **b–d** Normalized field distributions $|H_z|$ at the incident wavelengths of 11.625 (Mode 1), 10 (off-resonance) and 9.2 μm (Mode 2). The *white arrows* denote the input direction
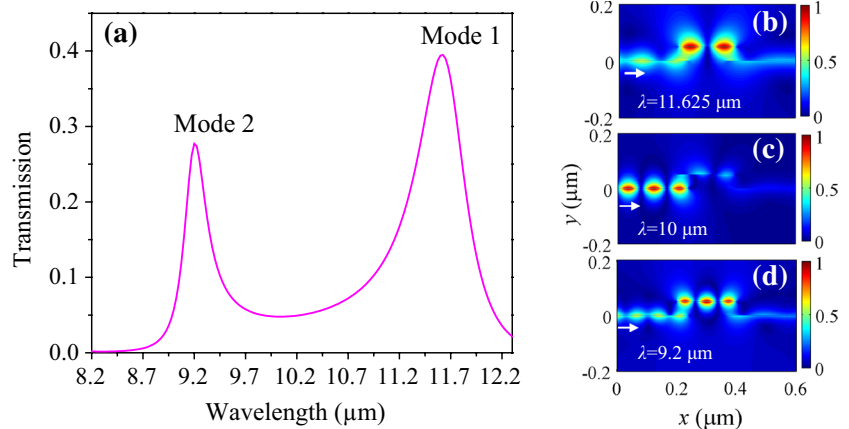


monolayer graphene embedded in the dielectric medium, the effective refractive index $n_{eff}$ of the excited SPP mode in the graphene can be described by the dispersion equation [33],

$$n_{eff} = \sqrt{\varepsilon_r - \left(\frac{2\varepsilon_r}{\sigma_g \eta_0}\right)^2} \quad (2)$$

Here, $\eta_0 \approx 377\ \Omega$ is the impedance of air. Figure 1b depicts the real part of $n_{eff}$ for the SPP mode supported by a single graphene layer freestanding in air ($\varepsilon_r = 1$). The numerical simulations are consistent with the theoretical curves obtained from Eq. (2). The numerical results are calculated using the commercial finite-element method software COMSOL Multiphysics.

## 3 Simulation results and analysis

Plasmonic oscillations emerging in graphene ribbons are increasingly acting as one of the most important and promising effects for the manipulation of optical features in graphene systems [22–24, 32]. The excitation of plasmonic resonance in graphene ribbons has been mainly focused on graphene ribbon arrays [23, 24, 32]. To further miniaturize GP devices, we utilize a coupling mechanism to realize plasmonic resonance in a single graphene nanoribbon. When the graphene sheets spatially approach each other, a strong optical coupling behavior occurs [33, 35]. By means of this near-field coupling between the graphene sheet and ribbon, the plasmonic resonance of the graphene ribbon can be excited in our configuration. The graphene ribbon can be treated as a coupled nanoresonator, which can be utilized to control the optical spectral response in the graphene system. In the study, the geometrical parameters of the graphene system are assumed as $W = 200$ nm, $d = 40$ nm and $g = 50$ nm. The chemical potential of the graphene ribbon is denoted by $\mu_c^*$ and also set as 0.15 eV.

For the sake of simplicity, the surrounding dielectric of graphene is assumed as $\varepsilon_r = 1$ [33, 35]. As depicted in Fig. 2a, the transmission spectrum of the graphene nanostructure is calculated through $T = P_{out}/P_{in}$, where $P_{out}$ and $P_{in}$ are the output and input powers of the light, respectively. The distance between the input and output ports is set as 600 nm. It exhibits obvious multiple peaks that result from multiple plasmonic resonant modes in the graphene nanoribbon. To further verify it, we plot the normalized field distributions $|H_z|$ at the peak wavelengths (11.625 and 9.2 μm) as well as a low-transmission position (10 μm), as shown in Fig. 2b–d. It is found that dipole and quadrupole modes are established in the graphene ribbon at the transmission peak wavelengths (i.e., Mode 1 and Mode 2). The resonance induces the light power output from the right graphene sheet. However, we cannot observe this performance at the low-transmission wavelength, where the graphene ribbon is under off-resonance condition. The asymmetric field perpendicular to the output graphene layer would not affect the calculation of transmission.

The resonance wavelength of the monolayer graphene ribbon is dependent on the ribbon width and chemical potential [32]. The plasmonic oscillation in graphene ribbons can be analyzed by the quasi-static analysis [23, 24, 32]. Combining with the Drude-like model, we can obtain an analytical expression of the resonance wavelength [24],

$$\lambda_p \approx \frac{2\pi \hbar c}{e} \sqrt{\frac{\varepsilon_r \varepsilon_0 \pi \eta W}{\chi \mu_c^*}}. \quad (3)$$

Here, $\eta$ is dimensionless constant, which can be deduced from the numerical simulations. $c$ is the velocity of light in vacuum. For a freestanding graphene ribbon, the introduced factor $\chi = 1/\varepsilon_r = 1$ [22]. In Fig. 3, we calculate the wavelengths of the resonance peaks for the different chemical potential $\mu_c^*$ and width $W$ of the graphene ribbon in our configuration by the numerical modeling and theoretical analysis. From the numerical results, the fitting values of $\eta$
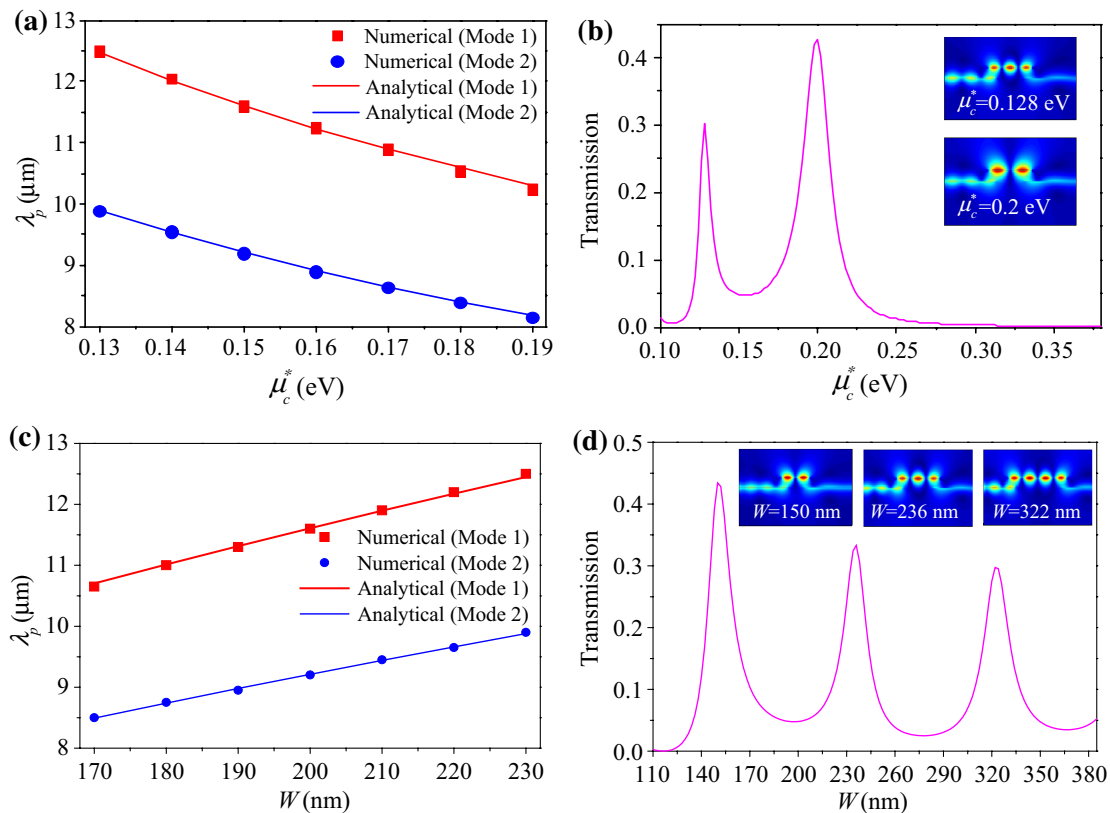
**Fig. 3** **a** Numerical modeling and analytical results of the resonance wavelength as a function of the chemical potential $\mu_c^*$ in the biased graphene ribbon. **b** Transmission values at the wavelength of 10 μm in the graphene system with different $\mu_c^*$. The insets show the field distributions $|H_z|$ for maximal transmission values at $\mu_c^* = 0.128$ and 0.2 eV. Here, $d = 40$ nm, $g = 50$ nm and $W = 200$ nm. **c** Numerical and analytical results of the resonance wavelengths versus the ribbon width $W$. **d** Transmission versus the different $W$ at the wavelength of 10 μm. The insets depict the field distributions $|H_z|$ for transmission peaks with $W = 150$, 236 and 322 nm. Here, $d = 40$ nm, $g = 50$ nm and $\mu_c^* = 0.15$ eV

for Mode 1 and Mode 2 are deduced to be 0.378 and 0.237, respectively. As shown in Fig. 3a, the resonance peak wavelength as a function of the chemical potential possesses a blue shift for higher $\mu_c^*$. The analytical results are in good agreement with the numerical modeling. It is worth noting that $\mu_c^*$ could be controlled by the external electronic voltage [21], as shown in Fig. 1a. Successively, we demonstrate the dependence of plasmonic transmission on $\mu_c^*$ at the fixed wavelength of 10 μm. We find that the transmission exhibits two maximal values with increasing $\mu_c^*$ from 0.1 to 0.38 eV, as shown in Fig. 3b. The plasmonic oscillations in the graphene ribbon contribute to the maximal transmission values at $\mu_c^* = 0.128$ and 0.2 eV, as shown in the insets of Fig. 3b. These results can be explained in terms of the resonant condition, which can be reasonably described as: $2Re\ (k_{SPP})W + \theta = 2\ m\pi$ [27, 40]. Here, $m$ is a natural number and stands for the order of the resonant mode, and $\theta$ is the additional phase shift from the edge ends of the graphene ribbon. In practice, the graphene with a finite size has two edge types (zigzag and armchair) [43]. Although the electronic spectrum would be modified by the

microscopic structure of graphene edges, plasmonics is the collective excitation of total electronic charges [42]. Moreover, the microscopic details of the graphene edge (zigzag or armchair) play a role only for the configurations with the sizes smaller than 10–20 nm [39]. Here, we also neglect the influence of different graphene edges, even though it may produce a certain modification for the SPP coupling. Combining the Drude-like model with the dispersion equation, the propagation constant of the SPP mode in a monolayer graphene can be derived as

$$k_{SPP} \approx \frac{8\pi^3\hbar^2 c\varepsilon_r}{e^2\mu_c^*\eta_0\lambda^2} + \frac{4\pi^2\hbar^2\varepsilon_r}{e^2\mu_c^*\eta_0\tau\lambda}i. \tag{4}$$

Here, the real part of $k_{SPP}$ is inversely proportional to the chemical potential and operating wavelength. Thereby, the larger chemical potential corresponds to the shorter wavelength for a certain resonant mode. The imaginary part of $k_{SPP}$ representing the loss of plasmonic mode is also in contrast to the chemical potential, which contributes to the ascending maxima for the larger chemical potential in the graphene ribbon, as can be seen in Fig. 3b.

According to the resonant condition, the graphene ribbon width $W$ is also an important factor to determine the plasmonic resonance wavelength. The numerical results in Fig. 3c show that the resonance peak wavelength has a red shift with increasing $W$. The numerical modeling is in accordance with the analytical results obtained from Eq. (3). Figure 3d depicts the transmission at the operating wavelength of 10 μm for different ribbon widths. Three maxima observed in the insets of Fig. 3d correspond to three different plasmonic resonant states. From the resonant condition, the theoretical separation between the adjacent maxima can be derived as $\Delta W = \lambda/(2n_{eff})$. Thus, $\Delta W$ is ~88 nm at the wavelength of 10 μm. The obtained separation $\Delta W = 86$ nm agrees well with the theoretical result. Because of the raised loss for a larger ribbon width, the maximal value decreases with the increase of $W$, as can be seen in Fig. 3d.

For the resonator-coupled waveguide system, the coupling strength plays a crucial role in the tailoring of the resonant features [44]. In the graphene system, the coupling distance $g$ controls the coupling strength between the graphene ribbon and graphene sheets. The larger $g$ corresponds to the weaker coupling strength [33, 35]. Figure 4a shows the transmission spectra for different coupling distances in the graphene configuration with $W = 236$ nm, $d = 40$ nm and $\mu_c^* = 0.15$ eV. A larger coupling distance induces a higher quality factor (narrower spectral bandwidth), while a reducing peak transmission. The quality factor of the resonator-coupled waveguide can be obtained from $Q = \lambda_0/\Delta\lambda$, where $\lambda_0$ and $\Delta\lambda$ are the central wavelength and full-width at half-maximum (FWHM) of the transmission peak, respectively. There exists a trade-off between the peak transmission and quality factor, as shown in Fig. 4b. The adjustment of the coupling distance offers a convenient scheme to control the quality factor of the plasmonic resonant response. The peak transmission becomes low enough when $g > 80$ nm, which is attributed to the nanoscale field confinement of mid-infrared SPP waves in the graphene [33, 35]. The dispersion and loss in the graphene give rise to the asymmetric profile and the transmission peak less than unity. Without considering the two factors, the transmission features near the resonance wavelength of the graphene ribbon can be analyzed by using coupled-mode theory and simply described as $T = (\kappa_\omega)^2/[(\omega-\omega_0)^2 + (\kappa_\omega + \kappa_i)^2]$ [44]. Here, $\omega$ is the incident frequency and $\omega_0$ represents the resonance frequency of graphene ribbon. $\kappa_i$ and $\kappa_\omega$ stand for the decay rates of the field due to the loss in the graphene ribbon and the power escape into the graphene sheets from the graphene ribbon, respectively. If coupling to graphene sheets were the only decay pathway for the ribbon power (i.e., $\kappa_i = 0$), the spatially coupling distance $g$ would enable the realization of a high quality factor while retaining a fixed peak transmission.
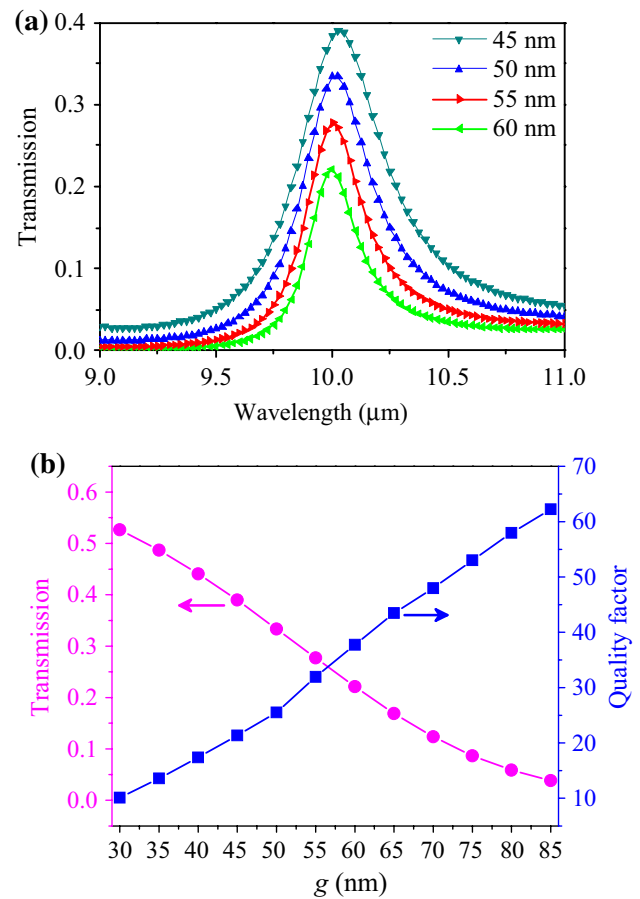


**(a)**

**(b)**

**Fig. 4** **a** Transmission spectra with different coupling distances $g$ between the graphene ribbon and graphene sheets. **b** Peak transmission and quality factor of the resonant spectrum for different $g$. Here, $W = 236$ nm, $d = 40$ nm and $\mu_c^* = 0.15$ eV

However, the decay channel $\kappa_i$ possesses nearly invariable as only $g$ is changed, while the decay rate $\kappa_\omega$ will intensively decrease when $g$ increases. The on-resonance transmission accordingly decreases. Meanwhile, the FWHM of the resonance peak $\Delta\lambda \approx 4\pi c(\kappa_\omega + \kappa_i)/\omega_0^2$ will decrease with $\kappa_\omega$. Thus, the quality factor of the resonance peak increases for the larger $g$, as shown in Fig. 4b. The plasmonic oscillation based on the graphene structure enables the realization of the tunable nanoscale mid-infrared filtering and switching elements.

It is worth noting that the system loss includes the graphene intrinsic loss and coupling waveguide loss. Due to the oscillation of the SPP wave in the graphene ribbon, it is difficult to obtain the graphene intrinsic loss in the system. Despite this, the following method may provide a feasible way. According to the dispersion relation of the graphene, the propagation constant of the plasmonic wave can be approximated as: $k_{spp} = k_0[2\pi\hbar^2\varepsilon_r(\omega + i\tau^{-1})]/(\eta_0 e^2\mu_c)$. Here, $k_0$ is the wave vector of light in vacuum. The graphene absorption derives from the imaginary part of $k_{spp}$. If
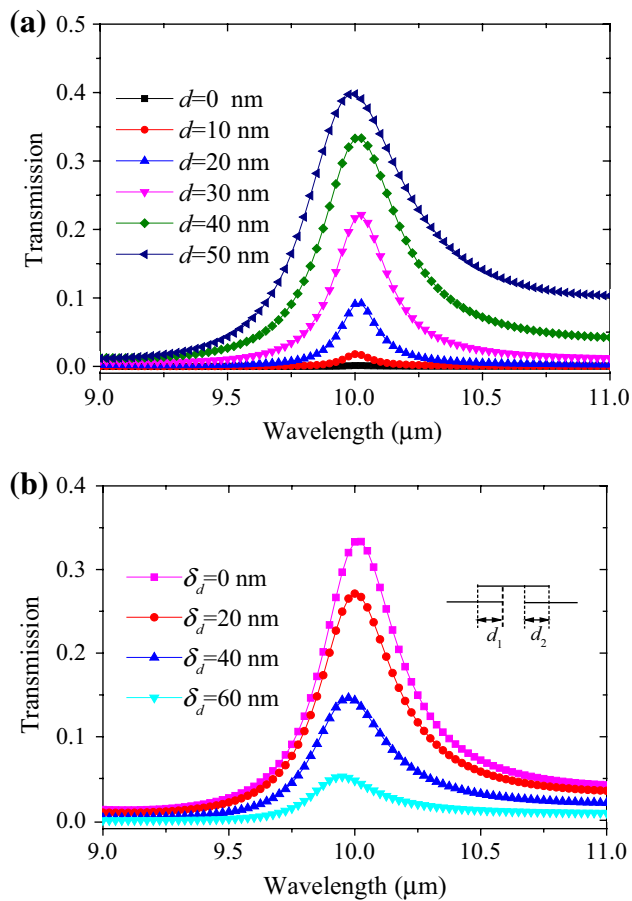
**(a)**



**(b)**



**Fig. 5** **a** Transmission spectra with different lengths $d$ of the overlaps between the graphene ribbon and graphene sheets. **b** Transmission spectra with different asymmetry degrees of the graphene waveguide. The inset shows the simplified profile of the graphene structure with the overlap lengths $d_1$ and $d_2$. In the calculations, the parameters are set as $W = 236$ nm, $g = 50$ nm, $d_1 + d_2 = 80$ nm and $\mu_c^* = 0.15$ eV

$\tau^{-1}$ is assumed to be small enough, thus, the obtained loss would mainly result from the waveguide coupling. Thus, the intrinsic loss could be achieved by subtracting the coupling loss from the total loss. The similar operation was utilized to study the effect of metal intrinsic loss on transmission features in metal waveguides [10].

Subsequently, we study the influence of the overlap length $d$ on the resonant transmission characteristics. In the structure, the parameters are set as $W = 236$ nm, $g = 50$ nm and $\mu_c^* = 0.15$ eV. It is shown in Fig. 5a that $d$ will affect the performance of the SPP transmission. Due to the decrease of the coupling decay rate $\kappa_\omega$, the transmission peak goes down with the decrease of $d$. The resonant coupling of the graphene ribbon nearly disappears when $d = 0$ nm. When $d$ is adjusted from 0 to 50 nm, meanwhile, the resonant position remains unchanged due to the fixed width of the graphene ribbon. To investigate the dependence of the transmission on the broken symmetry

of graphene coupling, we redefine the length of the overlap between the graphene sheets and graphene ribbon, as depicted in the inset of Fig. 5b. The asymmetric degree is defined as $\delta_d = d_1 - d_2$. Here, the parameters are assumed as $W = 236$ nm, $g = 50$ nm, $d_1 + d_2 = 80$ nm and $\mu_c^* = 0.15$ eV. It is found that the resonant transmission is suppressed when the geometric symmetry is broken.

## 4 Conclusions

In conclusion, we have numerically and theoretically investigated the plasmonic resonant effect and propagation characteristics in a nanoscale graphene waveguide system consisting of a monolayer graphene nanoribbon coupled with two guided-wave graphene sheets. The physical parameters such as the chemical potential and width of the graphene ribbon can effectively control the plasmonic spectral performances. The coupling strength between the graphene ribbon and graphene sheets determines the peak transmission and quality factor of the plasmonic resonance. The resonance transmission is also dependent on the coupling symmetry and the overlap length between the graphene ribbon and graphene sheets. We believe that these results could provide a new way toward the realization of nanoscale midinfrared spectral control and graphene plasmonic devices, especially the wavelength filtering and switching elements.

## References

1. W.L. Barnes, A. Dereux, T.W. Ebbesen, Surface plasmon subwavelength optics. Nature **424**, 824–830 (2003)
2. S.I. Bozhevolnyi, V.S. Volkov, E. Devaux, J.Y. Laluet, T.W. Ebbesen, Channel plasmon subwavelength waveguide components including interferometers and ring resonators. Nature **440**, 508–511 (2006)
3. H. Lu, X. Liu, L. Wang, Y. Gong, D. Mao, Ultrafast all-optical switching in nanoplasmonic waveguide with Kerr nonlinear resonator. Opt. Express **19**, 2910 (2011)
4. M. Ren, B. Jia, J.Y. Ou, E. Plum, J. Zhang, K.F. MacDonald, A.E. Nikolaenko, J. Xu, M. Gu, N.I. Zheludev, Nanostructured plasmonic medium for terahertz bandwidth all-optical switching. Adv. Mater. **23**, 5540–5544 (2011)
5. F. Bleckmann, E. Maibach, S. Cordes, T.E. Umbach, K. Meerholz, S. Linden, Photochromic switching of fano resonances in metallic photonic crystal slabs. Adv. Optical Mater. (2014). doi:10.1002/adom.201400187

6. Q. Gan, Y. Ding, F. Bartoli, 'Rainbow' trapping and releasing at telecommunication wavelengths. Phys. Rev. Lett. **102**, 056801 (2009)

7. H. Lu, X. Liu, Y. Gong, D. Mao, L. Wang, Enhancement of transmission efficiency of nanoplasmonic wavelength demultiplexer based on channel drop filters and reflection nanocavities. Opt. Express **19**, 12885–12890 (2011)

8. S. Dai, D. Zhao, Q. Li, M. Qiu, Double-sided polarization-independent plasmonic absorber at near-infrared region. Opt. Express **21**, 13125–13133 (2013)

9. W. Zhang, Q. Li, M. Qiu, A plasmon ruler based on nanoscale photothermal effect. Opt. Express **21**, 172–181 (2013)

10. H. Lu, X. Liu, D. Mao, Plasmonic analog of electromagnetically induced transparency in multi-nanoresonator-coupled waveguide systems. Phys. Rev. A **85**, 053803 (2012)

11. I.D. Leon, P. Berini, Amplification of long-range surface plasmons by a dipolar gain medium. Nat. Photonics **4**, 382–387 (2010)

12. H. Lu, X. Liu, G. Wang, D. Mao, Tunable high-channel-count bandpass plasmonic filters based on an analogue of electromagnetically induced transparency. Nanotechnology **23**, 444003 (2012)

13. Y. Gong, X. Liu, L. Wang, High-channel-count plasmonic filter with the metal–insulator–metal fibonacci-sequence gratings. Opt. Lett. **35**, 285–287 (2010)

14. H. Lu, X. Liu, D. Mao, L. Wang, Y. Gong, Tunable band-pass plasmonic waveguide filters with nanodisk resonators. Opt. Express **18**, 17922–17927 (2010)

15. Y. Zhang, N. Stokes, B. Jia, S. Fan, M. Gu, Towards ultra-thin plasmonic silicon wafer solar cells with minimized efficiency loss. Sci. Rep. **4**, 4939 (2013)

16. H. Lu, X. Liu, D. Mao, G. Wang, Plasmonic nanosensor based on fano resonance in waveguide-coupled resonators. Opt. Lett. **37**, 3780–3782 (2012)

17. A. Geim, K. Novoselov, The rise of graphene. Nat. Mater. **6**, 183–191 (2007)

18. K.S. Novoselov, A.K. Geim, S.V. Morozov, D. Jiang, Y. Zhang, S.V. Dubonos, I.V. Grigorieva, A.A. Firsov, Electric field effect in atomically thin carbon films. Science **306**, 666–669 (2004)

19. F. Bonaccorso, Z. Sun, T. Hasan, A.C. Ferrari, Graphene photonics and optoelectronics. Nat. Photonics **4**, 611–622 (2010)

20. Q. Bao, H. Zhang, B. Wang, Z. Ni, C.H.Y.X. Lim, Y. Wang, D.Y. Tang, K.P. Loh, Broadband graphene polarizer. Nat. Photonics **5**, 411 (2011)

21. A. Vakil, N. Engheta, Transformation optics using graphene. Science **332**, 1291–1294 (2011)

22. J. Christensen, A. Manjavacas, S. Thongrattanasiri, F.H.L. Koppens, F.J.G. de Abajo, Graphene plasmon waveguiding and hybridization in individual and paired nanoribbons. ACS Nano **6**, 431–440 (2012)

23. L. Ju, B. Geng, J. Horng, C. Girit, M. Martin, Z. Hao, H.A. Bechtel, X. Liang, A. Zettl, Y.R. Shen, F. Wang, Graphene plasmonics for tunable terahertz metamaterials. Nat. Nanotechnol. **6**, 630–634 (2011)

24. H. Chu, C. Gan, Active plasmonic switching at mid-infrared wavelengths with graphene ribbon arrays. Appl. Phys. Lett. **102**, 231107 (2013)

25. S. Thongrattanasiri, F.H.L. Koppens, F. Javier Garcı´a de Abajo, "Complete optical absorption in periodically patterned graphene". Phys. Rev. Lett. **108**, 047401 (2012)

26. Z. Fei, G. Andreev, W. Bao, L.M. Zhang, A.S. McLeod, C. Wang, M.K. Stewart, Z. Zhao, G. Dominguez, M. Thiemens, M.M. Fogler, M.J. Tauber, A.H. Castro-Neto, C.N. Lau, F. Keilmann, D.N. Basov, Infrared nanoscopy of dirac plasmons at the graphene-SiO$_2$ interface. Nano Lett. **11**, 4701–4705 (2011)

27. V.W. Brar, M. Jang, M. Sherrott, J.J. Lopez, H.A. Atwater, Highly confined tunable mid-infrared plasmonics in graphene nanoresonators. Nano Lett. **13**, 2541–2547 (2013)

28. F.H.L. Koppens, D.E. Chang, F.J. García de Abajo, Graphene plasmonics: A platform for strong light-matter interactions. Nano Lett. **11**, 3370–3377 (2011)

29. K.F. Mak, M.Y. Sfeir, Y. Wu, C.H. Lui, J.A. Misewich, T.F. Heinz, Measurement of the optical conductivity of graphene. Phys. Rev. Lett. **101**, 196405 (2008)

30. A.N. Grigorenko, M. Polini, K.S. Novoselov, Graphene plasmonics. Nat. Photonics **6**, 749–758 (2012)

31. B. Wang, X. Zhang, F.J. Garcı´a-Vidal, X. Yuan, J. Teng, "Strong coupling of surface plasmon polaritons in monolayer graphene sheet arrays". Phys. Rev. Lett. **109**, 073901 (2012)

32. W. Gao, J. Shu, C. Qiu, Q. Xu, Excitation of plasmonic waves in graphene by guided-mode resonances. ACS Nano **6**, 7806–7813 (2012)

33. B. Wang, X. Zhang, X. Yuan, J. Teng, Optical coupling of surface plasmons between graphene sheets. Appl. Phys. Lett. **100**, 131111 (2012)

34. G. Wang, X.M. Liu, H. Lu, C. Zeng, Graphene plasmonic lens for manipulating energy flow. Sci. Rep. **4**, 4073 (2014)

35. C. Gan, H. Chu, E. Li, Synthesis of highly confined surface plasmon modes with doped graphene sheets in the midinfrared and terahertz frequencies. Phys. Rev. B **85**, 125431 (2012)

36. P. Liu, W. Cai, L. Wang, X. Zhang, J. Xu, Tunable terahertz optical antennas based on graphene ring structures. Appl. Phys. Lett. **100**, 153111 (2012)

37. P.Y. Chen, A. Alù, Atomically thin surface cloak using graphene monolayers. ACS Nano **5**, 5855–5863 (2011)

38. C. Gan, Analysis of surface plasmon excitation at terahertz frequencies with highly doped graphene sheets via attenuated total reflection. Appl. Phys. Lett. **101**, 111609 (2012)

39. J. Garcia-Pomar, A. Nikitin, L. Martin-Moreno, Scattering of graphene plasmons by defects in the graphene sheet. ACS Nano **7**, 4988 (2013)

40. A.Y. Nikitin, T. Low, L. Martin-Moreno, Anomalous reflection phase of graphene plasmons and its influence on resonators. Phys. Rev. B **90**, 041407 (2014)

41. J. Chen, M. Nesterov, A. Nikitin, S. Thongrattanasiri, P. Alonso-Gonz´alez, T.M. Slipchenko, M. Ostler, T. Seyller, I. Crassee, F. Koppens, L. Martin-Moreno, J. Garcia de Abajo, A.B. Kuzmenko, R. Hillenbrand, "Strong plasmon reflection at nanometer-size gaps in monolayer graphene on SiC". Nano Lett. **13**, 6210 (2013)

42. AYu. Nikitin, F. Guinea, F.J. Garc´ıa-Vidal, L. Mart´ın-Moreno, "Edge and waveguide terahertz surface plasmon modes in graphene microribbons". Phys. Rev. B **84**, 161407(R) (2011)

43. F.J. Owens, Electronic and magnetic properties of armchair and zigzag graphene nanoribbons. J. Chem. Phys. **128**, 194701 (2008)

44. J. Joannopoulos, S. Johnson, J. Winn, and R. Meade, "Photonic crystals: Molding the flow of light," 2nd ed. Chap. 10, (Princeton Univ. Press, Princeton, 2008)